

Vietnam Academy of Science and Technology

# Vietnam Journal of Marine Science and Technology

journal homepage: vjs.ac.vn/index.php/jmst



Assessing the applicability of sentinel-2 remote sensing data to determine the bathymetry of a shallow coastal area: case study of Nhat Le Estuary, Quang Binh Province

Le Duc Hanh<sup>1</sup>, Hoang Thanh Son<sup>1,\*</sup>, Tong Phuc Tuan<sup>1</sup>, Vu Hai Dang<sup>2</sup>, Nguyen Ngoc Thang<sup>1</sup>, Bui Anh Tuan<sup>1</sup>, Tran Thai Binh<sup>3</sup>, Trinh Viet Nga<sup>4</sup>, Tran Anh Tuan<sup>2</sup>

Received: 12 May 2024; Accepted: 26 August 2024

### **ABSTRACT**

Seabed mapping is complex and expensive because it is often performed in a harsh environment sensitive to weather factors. To overcome these limitations, there have been many studies on the application of remote sensing data to measure the seabed depth based on physical laws about the attenuation of reflected energy of light when passing through a water column. The value of reflected energy from the seabed on remote sensing images is used to determine the depth of the seabed. Worldwide, studies have been conducted on applying remote sensing data to measure seabed depth through the modeling and GEE cloud computing platforms. There are also studies in Vietnam that map the seabed topography for offshore islands. This paper measured the seabed depth based on experimental data, survey lines conducted in April and October 2018, and Sentinel 2 remote sensing images data for Nhat Le estuary area. The paper aims to review and evaluate the correlation and accuracy of the application of Sentinel-2 remote sensing image data to measure the depth of the seabed topography for shallow coastal waters. The results show that the correlation coefficient R<sup>2</sup> along the surveyed lines is from 0.84 to 0.94, and the mean RMSE ranges from 0.70 to 0.74. The above assessment shows that surveyed lines that can be employed to interpret a larger area in the same satellite image scene using the empirical formula in the study area. The formula can also be used to determine the depth of bottom topography for other geographical areas with similarities in seawater turbidity and bottom material, as well as technical issues.

**Keywords:** Bathymetry, remote sensing, Nhat Le, Sentinel-2.

<sup>&</sup>lt;sup>1</sup>Institute of Geography, VAST, Vietnam

<sup>&</sup>lt;sup>2</sup>Institute of Marine Geology and Geophysics, VAST, Vietnam

<sup>&</sup>lt;sup>3</sup>HCMC Space Technology Application Center, Vietnam National Space Center, VAST, Vietnam
<sup>4</sup>Department of National Remote sensing, Ministry of Natural Resources and Environment, Hanoi, Vietnam

<sup>\*</sup>Corresponding author at: Institute of Geography, A27 Building, 18 Hoang Quoc Viet Road, Nghia Do Ward, Cau Giay District, Hanoi, Vietnam. *E-mail addresses*: htson@ies.vast.vn

### INTRODUCTION

Seabed topography is essential in marine research, socio-economic development planning, environment, and national security. The shallow coastal area is the place that is most strongly affected by the dynamic factors of the river and the sea (waves, currents, mud) and human activities.

The traditional method of mapping seabed topography is based on echo sounder mounted on ships combined with GPS devices [1]. This technique provides high spatial resolution but is expensive and weather-dependent. In a broad region, it is often considered less efficient.

Complementing the traditional method and partially overcoming the above limitations, remote sensing techniques for deep seabed topography have been developed using radar and optical data [2]. Radar imaging methods use backscatter to capture variations in water surface velocity and estimate water depth through interactions between tidal currents and seabed topography. However, radar data is heavily influenced by wind speed and is prone to noise; the results are often limited.

The optical bathymetry method is employed to determine the depth of the water column using the total radiant energy reflected by the water column [3]. The spectral bands of optical satellites (for example, the blue and green bands) are generally better at penetrating clear water. As solar radiation passes through the water, some are scattered and absorbed by the water and its components, and some is backscattered and recorded by multispectral sensors. Satellite-derived bathymetry is called water depth retrieval using multispectral imagery from satellites such as Landsat and Sentinel [4].

Throughout the last decade, many studies have been conducted on applying remote sensing data for deep seabed topography mapping worldwide [5–11] and in Vietnam [12–14].

El-Sayed (2018) [5] used Sentinel-2 and Landsat-8 images to map the bottom of Al Manzala Lake in Egypt. The study was implemented using blue and green bands for both sources of images. The computed depths were validated against in-situ data. The results

found that Sentinel-2 was more accurate than Landsat-8.

Traganos et al., (2018) [6] used a cloud computing platform to process Sentinel-2 satellite image data to create topographic maps of the seabed in three zones of the Aegean Sea. Spatial error maps reveal over-prediction over low-reflectance and shallow regions, and under-prediction over high-reflectance (< 6 m) and optically deep bottoms (> 17 m). This study also made the source code in Google Earth Engine available to the public.

In another study, Yunus et al., (2019) [7] used Sentinel-2 and Landsat-8 images to create seabed topographic maps of Florida - USA. The authors analyzed the suitability of Sentinel-2 and Landsat-8 imagery for bathymetric mapping of coastal and lake environments. Based on the availability of high-resolution LiDAR data for the study area, the bathymetric algorithm was built using an empirical approach and a Random Forest model. The results demonstrate that satellite imagery efficiently maps depths up to 10 m for coastal regions and up to 30 m for lakes.

Caballero and Stumpf (2020) [8] created topographic maps in two different seas, Florida and North Carolina, to examine the possibility of using a Sentinel-2 image for different turbidity area. The paper shows that using the Sentinel-2A/B's high revisit yields accurate satellite-derived bathymetry with median errors of less than 0.5 m for depths of 0–13 m when combined with LiDAR surveys.

In an attempt to combine different data sources, Thomas et al., (2021) [10] used ICESat-2 LiDAR data with Sentinel-2 optical imagery to create spatially continuous high-resolution bathymetric maps at regional-to-national scales in three areas: Florida, Crete, and Bermuda. ICESat-2 data were used to train the models. The study demonstrated good results when combining different sources of data to derive shallow water topography.

Duan et al., (2022) [11] recognized optical imagery's capability for depth retrieval. Using satellite-derived bathymetry, they explored the effectiveness of different models (machine learning and empirical inversion models) in depth retrieval from Landsat-8 and Sentinel-2A

images. The results show that given sufficient training data, the machine learning models was generally superior to that of the empirical inversion models. The models' bathymetry error increased sharply when the depth was more profound than 15 m.

Phan Quoc Yen et al., (2017) [12] used Landsat data to create the seabed topographic map of Truong Sa Lon Island. The result is a topographic map of the seabed up to 12 m deep with the model correlation coefficient  $R^2$  of 0.924; *RMSE* of 0.99 m. Nguyen Ha Phu et al., (2019) [13] used the WorldView-2 image, which is a high-resolution image, to create a seabed topographic map of Hai Sam Beach in the Truong Sa Islands by stereoscopic and photometric method. This method can reach a depth of 42 m based on stereoscopic imaging.

The above studies show that remote sensing data is being researched and widely applied to measure bottom topography. Few studies in Vietnam have mainly applied to offshore island areas without mentioning the applicability to coastal waters where dynamic regimes are complex and often affected by the inland alluvial flows passing through the estuaries. Therefore, this paper focuses on researching and evaluating the applicability of Sentinel-2 remote sensing data to measure the depth of seabed topography in shallow coastal areas, adopting experimental methods. The study area chosen is located in the Nhat Le area of Quang Binh province. The paper has evaluated the reliability and some limitations of the method.

### STUDY AREA

The study area is north of Nhat Le estuary, which belongs to Dong Hoi City, Quang Binh Province (Fig. 1). River-sea dynamics constantly influence this area, so the terrain changes constantly.

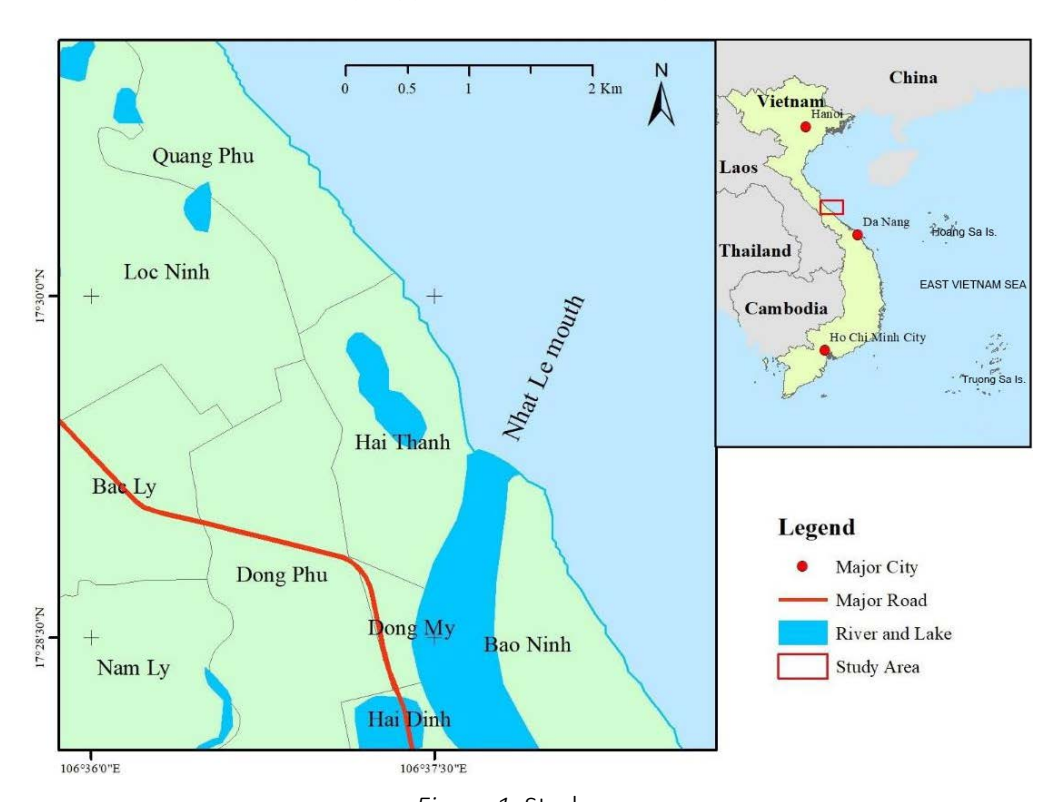


Figure 1. Study area

The study area has unconsolidated surface sediments belonging to the Quaternary system

(medium to fine sand). This sedimentary layer has poor cohesion and is susceptible to

fluctuations under the influence of exogenous marine dynamic processes such as waves, currents, and wind [15].

The average annual rainfall is 1,800-2,600 mm but unevenly distributed in space The rainy season usually time. concentrates on September - November, peaking in October. The rainfall in the rainy season accounts for 80-93% of the annual rainfall. The low rainy season usually occurs from January to April. Waves are an exogenous factor that directly affects the formation of the bottom topography. In winter, flood flows bring sand and mud from the river and meet high waves in the northeast direction perpendicular to the river mouth, creating a disputed area with weak dynamics and forming shoals in the estuary.

### **METHODOLOGIES AND DATASETS**

#### **Datasets**

The surveyed seabed topography data were carried out within the framework of the Bilateral project NDT.30.RU/17 hosted by the Institute of Geography in collaboration with the Russian Federation. Two surveys were performed at the end of April 2018 and October 2018 using echo sounders combined with GPS devices. We used the depth measurement points as experimental data. In the survey lines, the measuring points have been calibrated with tides and brought to the VN2000 projection. Sentinel-2 images employed in the study were on April 21, 2018, and October 23, 2018, which is close to the time of the depth measurement survey (Fig. 2).



Figure 2. Sentinel-2 images and survey lines in 21/4/2018 (left) and 23/10/2018 (right)

# Methodologies

Depth acquisition from optical remote sensing data is based on light attenuation when passing through water [16]. Shallow water absorbs less energy than deep water and thus has a higher reflectivity of solar radiation and vice versa [17]. At the same time, in shallower waters, the solar radiation reflected to the surface after hitting the bottom will be higher. Analytical equations convert the satellite sensor's water reflectance value into water depth.

However, this method's limitation is that a significant amount of energy must be reflected from the bottom surface. Therefore, it is only effective in shallow and clear waters since the reflectance value depends on the water column depth, and reflectance from the bottom surface and depends on the absorption and scattering properties of dissolved and suspended matter in the water column. Blue and green bands with wavelengths ranging from 400 to 600 nm and greater penetration capability are considered appropriate for depth estimation [18].

In this study, we used Sentinel-2 imagery in band 2 (Blue) and band 3 (Green) with wavelengths of 490 nm and 560 nm, respectively (Table 1).

Table 1. Characteristics of Sentinel-2 imagery

| Band | Center<br>wavelength (nm) | Band width (nm) | Spatial resolution (m) |
|------|---------------------------|-----------------|------------------------|
| 1    | 443                       | 20              | 60                     |
| 2    | 490                       | 65              | 10                     |
| 3    | 560                       | 35              | 10                     |
| 4    | 665                       | 30              | 10                     |
| 5    | 705                       | 15              | 20                     |
| 6    | 740                       | 15              | 20                     |
| 7    | 783                       | 20              | 20                     |
| 8    | 842                       | 115             | 10                     |
| 8b   | 865                       | 20              | 20                     |
| 9    | 945                       | 20              | 60                     |
| 10   | 1380                      | 30              | 60                     |
| 11   | 1610                      | 90              | 20                     |
| 12   | 2190                      | 180             | 20                     |

Survey data of depth have been calibrated for tides and waves and projected to the VN2000 coordinate system. Thus, in the following steps, performing tidal calibration during satellite image acquisition is unnecessary. We then selected 7 depth measurement lines for the experiment, of which 4 were used to build the correlation equation between remote sensing data and measured topographic data. The remaining 3 surveyed lines were used for accuracy assessment (Fig. 2). The surveyed lines

of the two field surveys are located close to each other to evaluate the applicability of remote sensing data in seabed topography mapping.

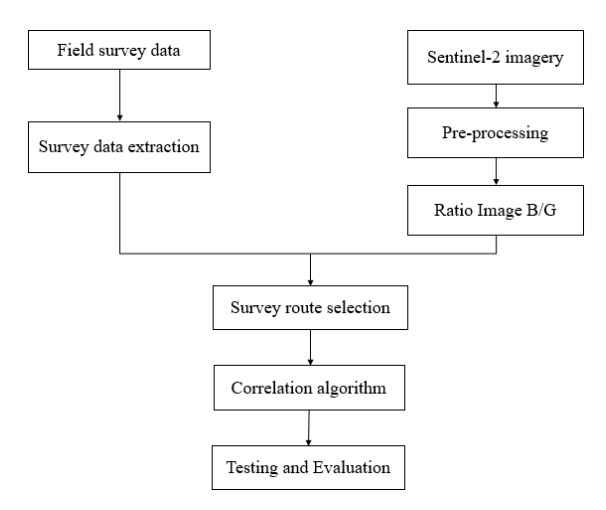


Figure 3. Flowchart of using remote sensing data for mapping seabed topography

Sentinel 2 images are selected and atmospherically corrected by the GEE cloud computing platform. The processed images were then exported to raster image files for further work in GIS software. The impact of sun-glint on the surface of the reflected waves bright fringes that affect the image interpretation. Therefore, it is necessary to eliminate the sun-glint effect [19].

$$R_i' = R_i - b_i \left( R_{NIR} - Min_{NIR} \right) \tag{1}$$

in which:  $R'_i$  is the pixel that was corrected for sun-glint in band I;  $R_i$  is the pixel of visible band I;  $b_i$  is the slope;  $R_{NIR}$  is the pixel value in band NIR;  $Min_{NIR}$  is the minimum value of NIR of samples.

Stumpf et al., (2003) [20] have provided widely used experimental algorithms that combine multiple regression and logarithmic scale regression of the blue and green bands. In his algorithm, the model that estimated the actual depth adopted the following formula:

$$Z = m_1 \frac{\ln(nR_w(\lambda_i))}{\ln(nR_w(\lambda_i))} - m_0$$
 (2)

in which: Z is the estimated depth;  $m_0$ ,  $m_1$  is the slope and intercept; n is the constant for the entire area;  $R_w$  is the reflectance value in band i or band j.

In GIS software, logarithm ratio image was created for each measurement

The depth measurement points combined with the corresponding logarithmic ratio satellite images were extracted to get Blue-Green logarithmic ratio values. Thus, each depth measurement point has 2 values: depth and Blue-Green logarithmic ratio (B/G).

Perform regression operations to calculate and evaluate accuracy at testing lines.

#### RESULTS AND DISCUSSION

Correlation charts between B/G values and the depth of surveyed points were built considered (Figs. 4–6). Optical remote sensing image signals in the aquatic environment depend on clouds, dust, water vapor, water

bubbles, turbidity, bottom material and even artificial floating objects [8]. Therefore these charts can be used to compare with the original image and remove noise to improve the accuracy of the regression algorithm.

The above charts clearly show correlation between B/G obtained from remote sensing data and in-situ bathymetry measurement, and further build up correlation parameters as follows.

## Regression

The regression was compiled based on insitu data of the surveyed lines 1,3,5,7 of the two field surveys in April 2018 (Date 1) and October 2018 (Date 2), and ratio image B/G derived from remote sensing data, we conducted the regression. The results are shown in Table 2.

Of all the functions (exponential, linear and quadratic function), we found that exponential function give highest correlation.

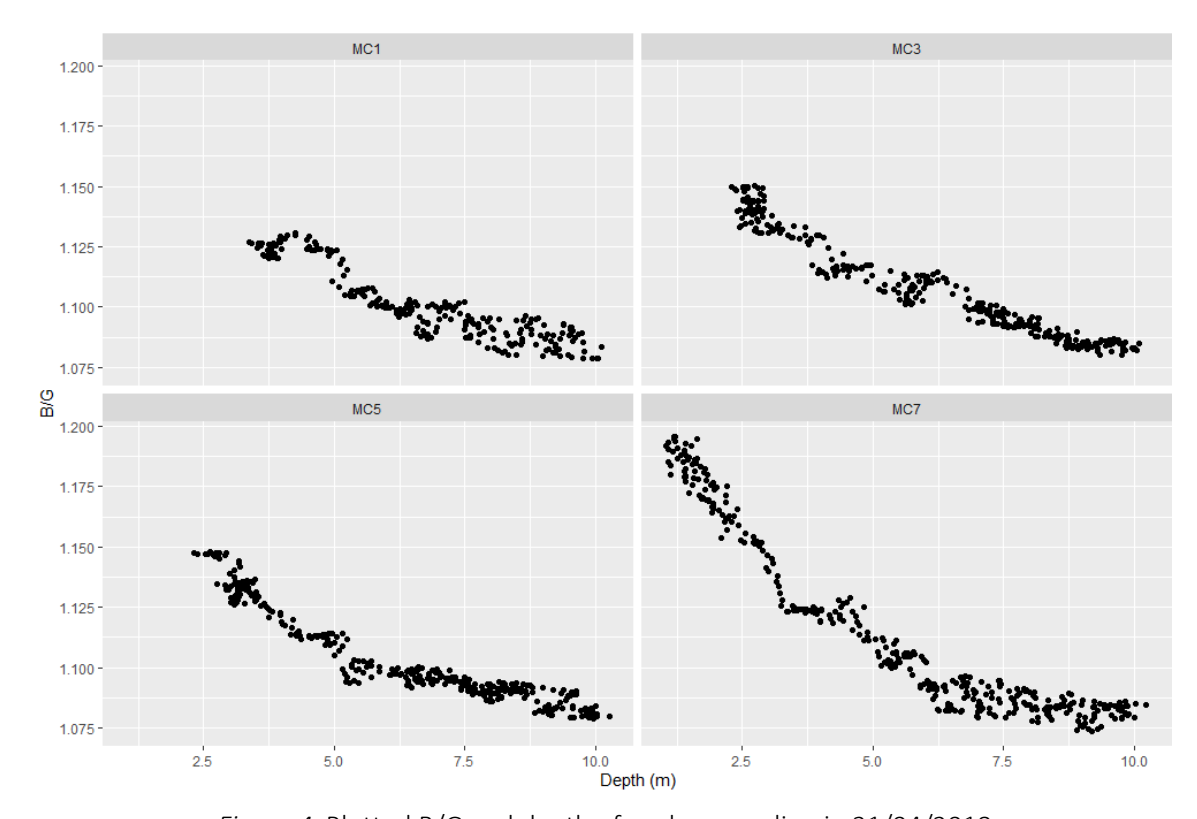


Figure 4. Plotted B/G and depth of each survey line in 21/04/2018

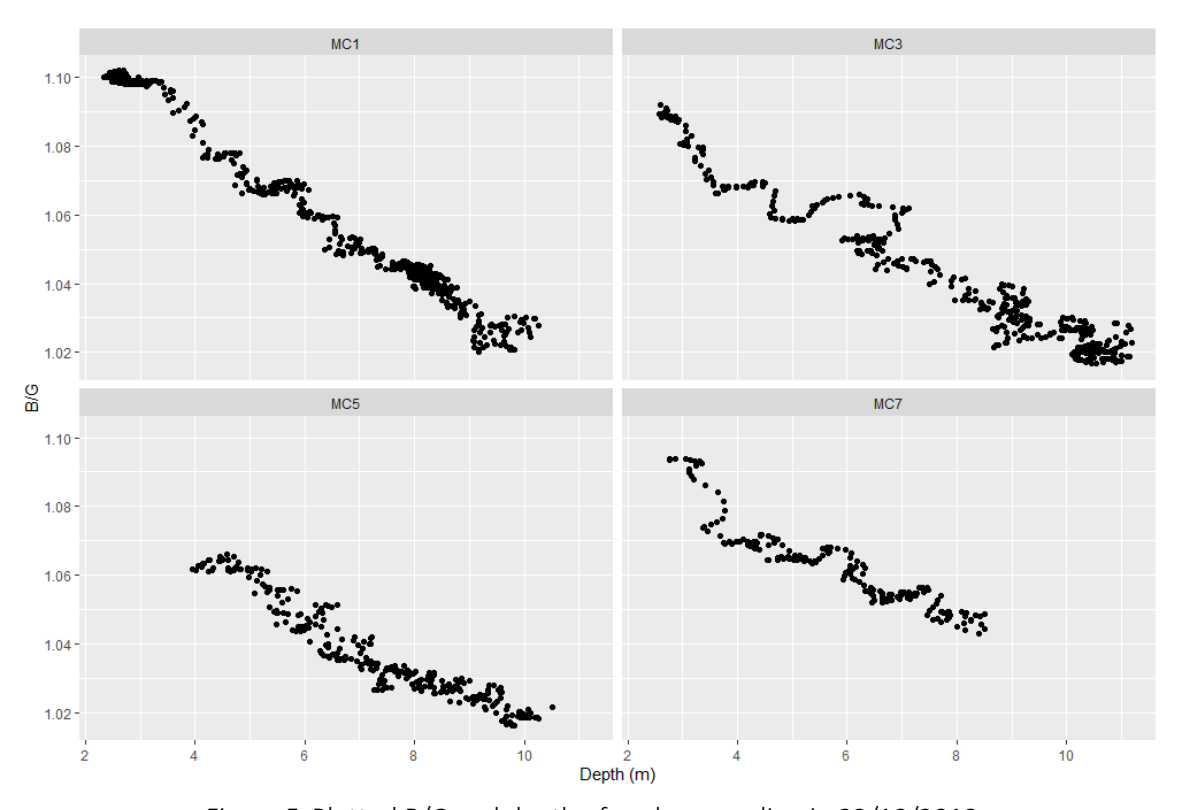


Figure 5. Plotted B/G and depth of each survey line in 23/10/2018

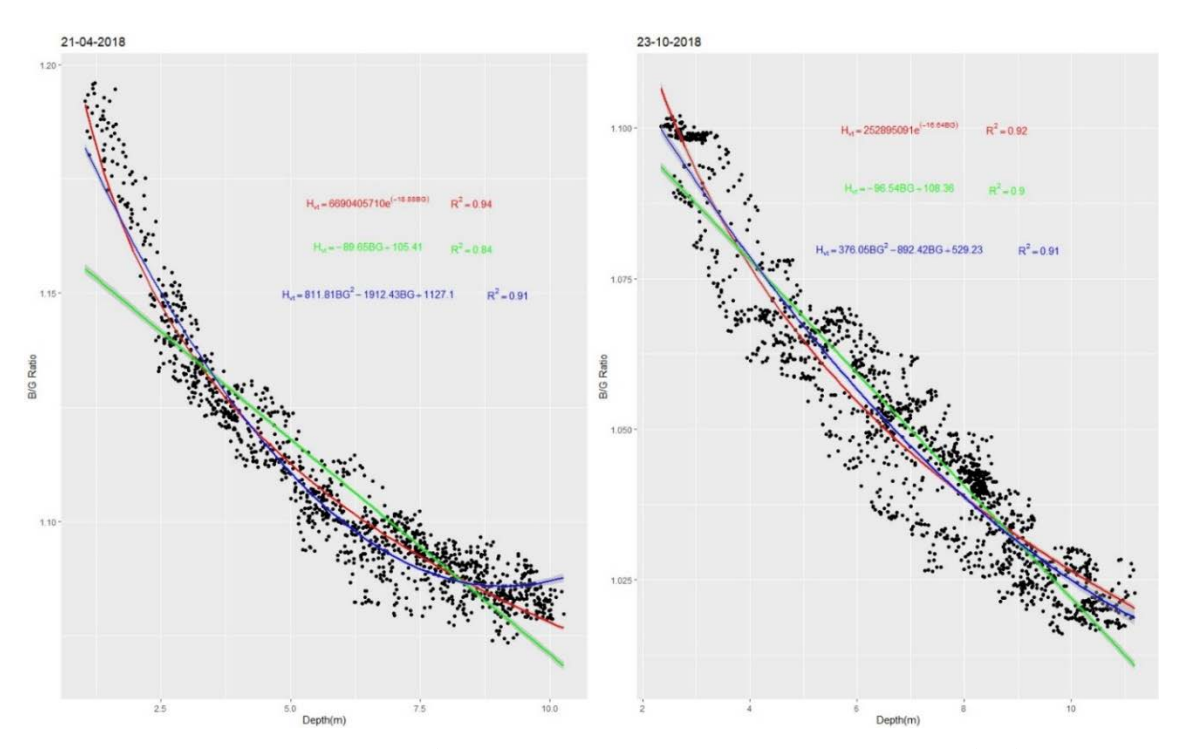


Figure 6. Correlation between B/G and depth of all 4 survey lines 1,3,5,7 in 21/04/2018 and 23/10/2018

Table 2. Equations established between B/G values and in-situ data

| Date 1               |   |              |  |  |  |
|----------------------|---|--------------|--|--|--|
| Exponential function | $H_{vt} = 6690405709.65 * e^{-18.88*BG}$      | $R^2 = 0.94$ |  |  |  |
| Linear function      | $H_{vt} = -89.65*BG + 105.41$                 | $R^2 = 0.84$ |  |  |  |
| Quadratic function   | $H_{vt} = 811.81*BG^2 - 1912.43*BG + 1127.91$ | $R^2 = 0.91$ |  |  |  |
| Date 2               |   |              |  |  |  |
| Exponential function | $H_{vt} = 252895090.91 * e^{-16.64*BG}$       | $R^2 = 0.92$ |  |  |  |
| Linear function      | $H_{vt} = -96.54*BG+108.36$                   | $R^2 = 0.90$ |  |  |  |
| Quadratic function   | $H_{vt} = 376.05*BG^2 - 892.42*BG + 529.23$   | $R^2 = 0.91$ |  |  |  |

in which:  $H_{vt}$ : estimated depth from remotely sensed data; BG: ratio Blue/Green image derived from remotely sensed data.

## Accuracy assessment

After building the correlation functions between depths and B/G of survey lines 1, 3, 5,

and 7 (Fig. 7), we used this function to calculate depth for survey lines 2, 4, and 6 and compared with the in-situ of these routes to assess the accuracy using *RMSE* and *MAE*.



Figure 7. Survey lines for expanding the testing area

$$RMSE = \sqrt{\frac{\sum (H_{td} - H_{vt})^{2}}{n}}$$

$$MAE = \frac{\sum (H_{td} - H_{vt})}{n}$$

in which: RMSE: root mean square error; MAE: mean absolute error;  $H_{td}$ : in-situ measurements;  $H_{vt}$ : estimated measurement from remotely sensed data.

The assessment results are shown in Table 3.

Table 3. Accuracy assessment

|                  | In-situ | Estimated depth based   | Estimated depth based | Estimated depth based |  |  |
|------------------|---------|-------------------------|-----------------------|-----------------------|--|--|
|                  | data    | on exponential function | on linear function    | on quadratic function |  |  |
| Date 1           |         |                         |                       |                       |  |  |
| Number of points | 947     | 947                     | 947                   | 947                   |  |  |
| $R^2$            |         | 0.94                    | 0.84                  | 0.91                  |  |  |
| RMSE             |         | 0.79                    | 0.91                  | 0.74                  |  |  |
| Max depth        | 10.29   | 10.25                   | 9.04                  | 10.21                 |  |  |
| Min depth        | 1.15    | 1.29                    | -0.79                 | 1.6                   |  |  |
| Mean depth       | 6.2     | 5.88                    | 5.95                  | 5.92                  |  |  |
| MAE              |         | 0.61                    | 0.71                  | 0.58                  |  |  |
| Date 2           |         |                         |                       |                       |  |  |
| Number of points | 1256    | 1256                    | 1256                  | 1256                  |  |  |
| $R^2$            |         | 0.92                    | 0.90                  | 0.91                  |  |  |
| RMSE             |         | 0.77                    | 0.73                  | 0.70                  |  |  |
| Max depth        | 11.21   | 11.74                   | 10.40                 | 10.89                 |  |  |
| Min depth        | 1.98    | 2.19                    | 0.67                  | 1.68                  |  |  |
| Mean depth       | 7.30    | 6.96                    | 6.91                  | 6.94                  |  |  |
| MAE              |         | 0.62                    | 0.60                  | 0.56                  |  |  |

## Expand the testing area

To consider the applicability of remote sensing data for seabed topography mapping, we conducted 3 survey lines for each Date in the south of Nhat Le estuary. The survey lines were conducted with the longest distance from Nhat Le estuary is 3 km, and reached deepest of 12 m. We then put the regression formulas into the survey lines to calculate and evaluate. The results are shown in Table 4.

Table 4. Accuracy assessment after expanding the testing area

|                  | In-situ | Estimated depth based   | Estimated depth based | Estimated depth based |  |  |
|------------------|---------|-------------------------|-----------------------|-----------------------|--|--|
|                  | data    | on exponential function | on linear function    | on quadratic function |  |  |
| Date 1           |         |                         |                       |                       |  |  |
| Number of points | 199     | 199                     | 199                   | 199                   |  |  |
| RMSE             |         | 1.29                    | 1.05                  | 1.22                  |  |  |
| Max depth        | 11.46   | 13.17                   | 10.23                 | 12.57                 |  |  |
| Min depth        | 1.99    | 2.4                     | 2.14                  | 2.15                  |  |  |
| Mean depth       | 7.12    | 8.02                    | 7.54                  | 7.99                  |  |  |
| MAE              |         | 1.04                    | 0.85                  | 1.00                  |  |  |
| Date 2           |         |                         |                       |                       |  |  |
| Number of points | 897     | 897                     | 897                   | 897                   |  |  |
| RMSE             |         | 2.31                    | 2.79                  | 2.35                  |  |  |
| Max depth        | 10.74   | 9.30                    | 9.05                  | 9.16                  |  |  |
| Min depth        | 3.55    | 1.08                    | -3.44                 | 0.09                  |  |  |
| Mean depth       | 7.26    | 5.14                    | 5.01                  | 5.18                  |  |  |
| MAE              |         | 2.12                    | 2.25                  | 2.08                  |  |  |

Table 4 shows that *RMSE* and *MAE* are all greater than those values in Table 3. Taking more detail for each Date, the error of the

survey line in April is less than in October and can be used for interpreting seabed bathymetry. To explain this, here are some causes:

Estuaries often have high fluctuations due to the hydro-litho-dynamic regime, which causes constant change of the seabed bathymetry over time.

The river flow carries suspended matter from inland to the estuary and then the ocean current carries that material along the two sides of the estuary. The amount of suspended matters on the two sides differs depending on certain situations during image acquisition.

April is the transitional time from dry to rainy seasons. Therefore, the amount of suspended matter and waves is smaller than that of October, the time of heavy rainfall and strong northeast monsoon, which creates large waves and coastal currents carrying material to the south. Therefore, there is a significant difference between the two sides of the river mouth, leading to a large error of *RMSE* and *MAE* in October.

#### Discussion

During the work implementation, some geographical and technical issues were identified that affected the applicability and improved the accuracy of the results.

The experimental depth measurement data is projected to the VN2000 projection system, which no longer depends on the tidal water level, making the depth calculation for seabed topographic mapping more convenient.

According to the above results, when the field measurements are close to the time of good-quality image acquisition, the *RMSE* and *MAE* errors are minor  $^{\sim}$  1.0, which can establish a seabed topographic map at a scale of 1/10,000.

This study used field measurements combined with remote sensing data in acquired in April and October 2018 and found that for different scenes. One equation to interpolate the seabed topography are different. One equation cannot be applied for the same study area for different image acquisition dates.

Sentinel-2 images with a frequency of 5 or 12 days and spatial resolution of 10 m are useful for exploitation and use to mapping seabed bathymetry. However, applying this to less steep areas at this spatial resolution is

better Assuming that the bathymetry map required isoline differences of 1 m and remote sensing cell size of 10x10 m, the appropriate slope must be less than 10%.

Although estuaries often have high fluctuations in the hydro-geo-dynamic regime, the paper points out that a closer correlation was obtained between the time of image acquisition and field trip bathymetry measurement.

Some methodology restrictions, due to optical remote sensing images, use the visible wavelength, so cloudy areas should be excluded to minimize the error of the correlation function. In addition, the seasonal alluvial flows are strongly affected because their mass absorbs almost the reflected light energy, making the methodology challenging to operate, as a result, it is only suitable for areas with relative transparency water and/or stable turbidity.

Waves change the water column's height, affecting the interpretation results. In addition, the water bubbles created by waves also affect the method's accuracy.

## CONCLUSION

Remote sensing data in seabed topography mapping is increasingly being studied and developed through model and cloud computing platforms. Sentinel-2 remote sensing data with a high temporal resolution (5 days) and high spatial resolution (10 m) are valuable resources for measuring the depth of seabed topography.

This study evaluates the applicability of Sentinel-2 remote sensing data in deep seabed topographic measurement by experimental method with data of 7 depth surveyed lines from two field surveys in April and October 2018, in which 4 lines were used to build correlation equations, 3 surveyed lines were used to test and evaluate. The results show that the regression equations have a reasonably high correlation coefficient from 0.84 to 0.94, *RMSE* error is 0.70–0.91 in the sea region north of Nhat Le estuary. When applying the regression equations obtained in the north area to the south area of Nhat Le estuary, the

*RMSE* of the regression equations is 0.85–1.04 for the April survey and 2.31–2.79 for the October survey.

The evaluation results show that we can use remote sensing images to supplement data for non-surveyed areas in particular conditions where it is not possible to conduct measurements and surveys with sufficient detail. At the same time, we can interpret seabed topography in other areas within the same remote-sensing image. Applicability is more effective for geographical areas with similar conditions regarding water quality (suspended matter) and bottom material. This study also presents several issues to be effects drawn about the causing measurement uncertainty to better apply to the bathymetry measurement method using remote sensing data.

Acknowledgements: This research was funded by the Project codes UQĐTCB.04/23–24 and VAST05.05/23-24 of the Vietnam Academy of Science and Technology (VAST).

## **REFERENCES**

- [1] Q. Guo, C. Fu, Y. Chen, and Y. Zhang, "Application of multi-beam bathymetry system in shallow water area," *Journal of Physics: Conference Series*, vol. 2428, no. 1, p. 012042, 2023. DOI: 10.1088/1742-6596/2428/1/012042.
- [2] J. Gao, "Bathymetric mapping by means of remote sensing: methods, accuracy and limitations," *Progress in Physical Geography*, vol. 33, no. 1, pp. 103–116, 2009. DOI: 10.1177/0309133309105657.
- [3] F. Eugenio, J. Marcello, and J. Martin, "High-resolution maps of bathymetry and benthic habitats in shallow-water environments using multispectral remote sensing imagery," *IEEE Transactions on Geoscience and Remote Sensing*, vol. 53, no. 7, pp. 3539–3549, 2015. DOI: 10.1109/TGRS.2014.2377300.
- [4] X. Guo, X. Jin, and S. Jin, "Shallow water bathymetry mapping from ICESat-2 and

- Sentinel-2 based on BP neural network model," *Water*, vol. 14, no. 23, p. 3862, 2022. DOI: 10.3390/w14233862.
- [5] M. S. El-Sayed, "Comparative study of satellite images performance in mapping lake bathymetry: Case study of Al-Manzala Lake, Egypt," *American Journal of Geographic Information System*, vol. 7, no. 3, pp. 82–87, 2018. DOI: 10.5923/j.ajgis.20180703.02.
- [6] D. Traganos, D. Poursanidis, B. Aggarwal, N. Chrysoulakis, and P. Reinartz, "Estimating satellite-derived bathymetry (SDB) with the Google Earth Engine and Sentinel-2," *Remote Sensing*, vol. 10, no. 6, p. 859, 2018. DOI: 10.3390/rs10060859.
- [7] A. P. Yunus, J. Dou, X. Song, and R. Avtar, "Improved bathymetric mapping of coastal and lake environments using Sentinel-2 and Landsat-8 images," *Sensors*, vol. 19, no. 12, p. 2788, 2019. DOI: 10.3390/s19122788.
- [8] I. Caballero and R. P. Stumpf, "Towards routine mapping of shallow bathymetry in environments with variable turbidity: Contribution of Sentinel-2A/B satellites mission," *Remote Sensing*, vol. 12, no. 3, p. 451, 020. DOI: 10.3390/rs12030451.
- [9] G. Casal, J. D. Hedley, X. Monteys, P. Harris, C. Cahalane, and T. McCarthy, "Satellitederived bathymetry in optically complex waters using a model inversion approach and Sentinel-2 data," *Estuarine, Coastal* and Shelf Science, vol. 241, p. 106814, 2020. DOI: 10.1016/j.ecss.2020.106814.
- [10] N. Thomas, A. P. Pertiwi, D. Traganos, D. Lagomasino, D. Poursanidis, S. Moreno, and L. Fatoyinbo, "Space-borne cloud-native satellite-derived bathymetry (SDB) models using ICESat-2 and Sentinel-2," *Geophysical Research Letters*, vol. 48, no. 6, e2020GL092170, 2021. DOI: 10.1029/2020GL092170.
- [11] Z. Duan, S. Chu, L. Cheng, C. Ji, M. Li, and W. Shen, "Satellite-derived bathymetry using Landsat-8 and Sentinel-2A images: assessment of atmospheric correction algorithms and depth derivation models in shallow waters," *Optics Express*, vol. 30,

- no. 3, pp. 3238–3261, 2022. DOI: 10.1364/OE.444557.
- [12] P. Q. Yen, D. K. Hoai, and D. T. B. Hoa, "Research on bathymetry mapping of shallow water areas around islands in the Spratly Archipelago using deep remote sensing technology," VNU Journal of Science: Earth and Environmental Sciences, vol. 33, no. 4, pp. 63–73, 2017. DOI: 10.25073/2588-1094/vnuees.4194.
- [13] V. T. Tran, and C. T. Diem, "Research on technical solutions using GNSS-RTK technology in the construction of super high-rise buildings in Vietnam," *Journal of Surveying and Cartography*, no. 42, pp. 39–43. DOI: 10.54491/jgac.2019.42.356.
- [14] T. T. Tung and D. N. Quang, "Analysing the causes of prolonged flooding in the Nhat Le river basin due to the historical flood in 2020," Journal of Water Resources & Environmental Engineering, vol. 81, pp. 82–90, 2022.
- [15] N. T. Hai, T. Nghi, and N. V. Bach, "Sedimentary characteristics and evolution of sand formations in the coastal strip of Quang Binh province," *Journal of Geology*, no. 281, pp. 30–40, 2004.
- [16] A. Pacheco, J. Horta, C. Loureiro, and Ó. Ferreira, "Retrieval of nearshore bathymetry from Landsat 8 images: A tool for coastal monitoring in shallow waters,"

- Remote Sensing of Environment, vol. 159, pp. 102–116, 2015. DOI: 10.1016/j.rse.2014.12.004.
- [17] A. Pope, T. A. Scambos, M. Moussavi, M. Tedesco, M. Willis, D. Shean, and S. Grigsby, "Estimating supraglacial lake depth in West Greenland using Landsat 8 and comparison with other multispectral methods," *The Cryosphere*, vol. 10, no. 1, pp. 15–27, 2016. DOI: 10.5194/tc-10-15-2016.
- [18] X. Monteys, P. Harris, S. Caloca and C. Cahalane, "Spatial prediction of coastal bathymetry based on multispectral satellite imagery and multibeam data," *Remote Sensing*, vol. 7, no. 10, pp. 13782–13806, 2015. DOI: 10.3390/rs71013782.
- [19] J. D. Hedley, A. R. Harborne and P. J. Mumby, "Simple and robust removal of sun glint for mapping shallow-water benthos," *International Journal of Remote Sensing*, vol. 26, no. 10, pp. 2107–2112, 2005. DOI: 10.1080/01431160500034086.
- [20] R. P. Stumpf, K. Holderied, and M. Sinclair, "Determination of water depth with high-resolution satellite imagery over variable bottom types," *Limnology and Oceanography*, vol. 48, no. 1, pt. 2, pp. 547–556, 2003. DOI: 10.4319/lo.2003.48.1\_part\_2.0547.